IOPscience iopscience.iop.org

Home Search Collections Journals About Contact us My IOPscience

Nanocomposite indium tin oxide thin films: formation induced by a large oxygen deficiency and properties

This article has been downloaded from IOPscience. Please scroll down to see the full text article.

2010 J. Phys.: Condens. Matter 22 045006

(http://iopscience.iop.org/0953-8984/22/4/045006)

View the table of contents for this issue, or go to the journal homepage for more

Download details:
IP Address: 129.252.86.83
The article was downloaded on 30/05/2010 at 06:37

Please note that terms and conditions apply.

J. Phys.: Condens. Matter **22** (2010) 045006 (7pp) doi:10.1088/0953-8984/22/4/045006

Nanocomposite indium tin oxide thin films: formation induced by a large oxygen deficiency and properties

M Nistor[1], J Perrière[2,4], C Hebert[2] and W Seiler[3]

[1] National Institute for Lasers, Plasma and Radiation Physics, Plasma Physics and Nuclear Fusion Laboratory, L22 PO Box MG-36, 77125 Bucharest-Magurele, Romania
[2] Institut des Nanosciences de Paris, Université Pierre et Marie Curie-Paris 6, CNRS UMR 7588, Campus Boucicaut, 140 rue de Lourmel, 75015 Paris, France
[3] LIM, ENSAM, UMR CNRS 8006, 151 Boulevard de l'Hopital, 75013 Paris, France

E-mail: jacques.perriere@insp.jussieu.fr

Received 25 September 2009, in final form 23 November 2009
Published 12 January 2010
Online at stacks.iop.org/JPhysCM/22/045006

Abstract
We report on the formation and properties of nanocomposite indium tin oxide thin films which are grown by pulsed-electron beam deposition under a low oxygen pressure leading to the formation of highly non-stoichiometric indium tin oxide films. For growth at room temperature these films are amorphous and insulating, while at higher temperatures, the oxygen deficiency leads to a disproportionation reaction with the formation of metallic clusters (indium or indium tin clusters) embedded in a stoichiometric crystalline indium tin oxide. This matrix is well crystallized and even epitaxial for growth on *c*-cut sapphire single crystal substrates. The presence of the metallic clusters induces specific transport properties, i.e. a metallic conductivity at room temperature followed by a superconducting transition at low temperature (about 6 K). Moreover, the solid–liquid and liquid–solid phase transitions in the metallic clusters can be clearly seen from the resistivity curves as a function of temperature (in the room temperature to 450 K range), through specific changes in resistivity and the appearance of a hysteresis cycle.

(Some figures in this article are in colour only in the electronic version)

1. Introduction

Owing to its specific properties, highly desirable for technological applications, i.e. high electrical conductivity ($\rho \sim 10^{-4}$ Ω cm) and high optical transparency in the visible wavelength range, tin-doped indium oxide (ITO) can be used in a wide variety of applications [1]. The growth of ITO thin films has thus been frequently studied by numerous methods, which showed that the structural characteristics and physical properties of ITO films are very sensitive to the growth conditions, and so the films can be either amorphous or polycrystalline, insulating or conductive, transparent or absorbing, as a function of the deposition parameters [2–4]. In particular the oxygen pressure during the growth, which determines the amount of oxygen atoms fixed in the growing films, has been found to play an important role in the physical properties of the films [5, 6]. Moreover, whatever the deposition methods, annealing treatments (in reducing or oxidizing atmosphere) are often applied to improve the structure and properties of the as deposited ITO films. As a matter of fact, films with very specific properties can be obtained [7, 8], and even the formation of metallic indium at the surface of the ITO films [9] has been reported.

As the stoichiometry of ITO films appears as one of the most pertinent parameters governing their nature and properties, we have studied the effects of oxygen deficiency in ITO films. The pulsed-electron beam deposition method (PED) was used to obtain such oxygen deficient ITO films. Indeed PED is based on the use of a pulsed beam of polyenergetic electrons to ablate a target material [10–12]. PED of oxide target in a reducing or neutral ambient gas would thus permit one to control the incorporation of oxygen, and to promote thus the formation of oxygen deficient oxide films [10].

[4] Author to whom any correspondence should be addressed.

 © 2010 IOP Publishing Ltd Printed in the UK

In this paper, we present the results concerning ITO films with large oxygen deficiencies (more than 20% of oxygen missing). Such large oxygen deficiencies induce the formation of nanocomposite films (metallic clusters in a stoichiometric matrix), via a disproportionation reaction of metastable ITO sub-oxides in a stoichiometric ITO matrix and metallic In or In–Sn clusters. The structural characteristics and physical properties of these nanocomposite films are presented. The epitaxial growth of the stoichiometric ITO matrix is observed, while very specific transport properties are associated with the presence of metallic clusters embedded in an insulating matrix. In addition, the behaviour of these metallic clusters as a function of temperature will be discussed, i.e. their solid to liquid phase transition is observed through changes in resistivity.

2. Experimental details

The ITO thin films (in the 80–190 nm range) were grown by the PED method on quartz and *c*-cut sapphire single-crystal substrates. In PED a pulsed-electron beam having a pulse width about 110 ns (FWHM) and 2.5 J cm^{-2} fluence, produced in a channel-spark discharge [10, 13], was used to ablate a rotating ITO target. The channel-spark discharge consists of a hollow cathode, a dielectric capillary tube (6 mm diameter and 100 mm length) and the vacuum chamber as the grounded anode. The external capacitor (C) was 16 nF and was discharged at a high voltage in the range 14–16 kV, with a frequency of 1–2 Hz. The substrate was heated from room temperature to 500 °C under an argon pressure kept at 2×10^{-2} mbar. After deposition, the films were cooled down in the ablation chamber under the argon pressure conditions used for the growth.

The thickness and composition of the films were determined by Rutherford backscattering spectrometry (RBS), using the 2 MeV Van de Graaff accelerator of the INSP. It has to be noted that owing to the limited mass resolution of the method, indium and tin cannot be separated using the RBS spectra. Thus, for the analysis, it was assumed that the target composition ($(In_{1.8}Sn_{0.2})O_3$) is maintained in the films. Moreover, the oxygen content was only determined with a 5% accuracy, due to the low RBS yield for light elements like oxygen.

The crystalline structure of the films was studied by x-ray diffraction analyses (XRD) using the Philips Xpert diffractometer at the INSP and at the ENSAM. The nature of the crystalline phases was studied by using diffraction either in the Bragg–Brentano mode or in the grazing incidence geometry, and by using asymmetric diffraction, i.e. pole figure measurements. In this last geometry, the epitaxial relationships between ITO films and single-crystal substrates were studied and the precise in-plane orientations between film and substrate were determined.

The transport properties (resistivity as a function of temperature from room T down to liquid He T) of the ITO films were obtained by the classical four-probe method.

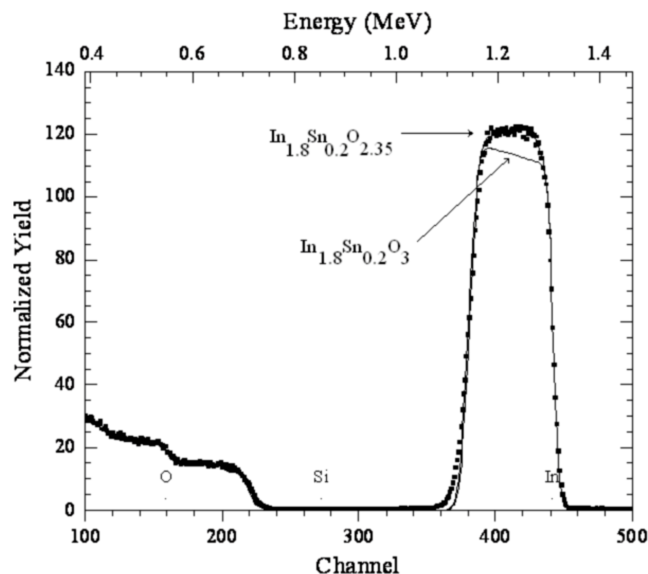

Figure 1. A typical RBS spectrum recorded for an ITO film grown by PED on a quartz substrate at 500 °C.

3. Results and interpretations

3.1. Film composition and morphology

During PED or other methods of growth of oxide films [14, 15], their stoichiometry may be controlled by the partial oxygen pressure during the growth. Indeed, the flux of oxygen atoms reaching the surface of the growing film depends upon the oxygen partial pressure (P_{O_2}), and as a result the incorporation of oxygen atoms is limited when P_{O_2} is decreased. In this work it was thus possible to change the oxygen concentration in the ITO films from their ideal stoichiometry ($(In_{1.8}Sn_{0.2})O_3$) down to a large oxygen deficiency ($(In_{1.8}Sn_{0.2})O_x$ with $x < 2.4$), by solely changing the O to Ar ratio in the working gas. In this paper, we will focus our attention on ITO films grown under pure argon at a pressure (2×10^{-2} mbar), corresponding to a low oxygen residual pressure ($<10^{-5}$ mbar).

Figure 1 represents a typical RBS spectrum recorded for an ITO thin film (142 nm) grown at 500 °C on a quartz substrate. Though large tails towards lower energies are not observed on the rear edge of the In (and Sn) contribution, the general shape of this RBS spectrum (broadening of the In rear edge and Si front edge) indicates some roughening. Note that whatever the nature, composition and properties of the materials to be deposited by the PED method, nanoparticulates (10–100 nm) are observed at the surface of the films [10]. In this work we tried to optimize the growth conditions to avoid this effect, as has been reported [10]; however, even if we reduced the importance of this effect, it was not possible to grow ITO films free from any particulates at their surface. This leads to the broadening of the various contributions observed in this RBS spectrum.

This RBS spectrum cannot be fitted with the ideal stoichiometric $(In_{1.8}Sn_{0.2})O_3$ composition. Indeed, the calculated RBS spectrum corresponding to this ideal stoichiometry is presented in figure 1, and shows the importance of this

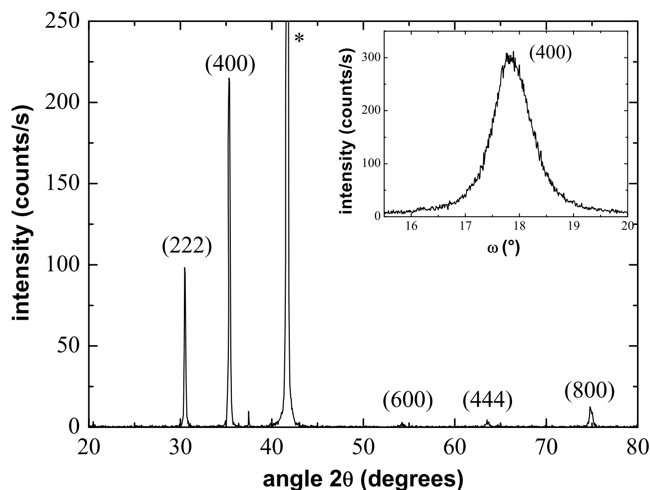

Figure 2. X-ray diffraction patterns for an ITO film grown by PED at 500 °C on a single-crystal *c*-cut sapphire substrate. The inset represents the rocking curve of the (400) reflection peak. The (00.6) sapphire substrate peak is marked with *.

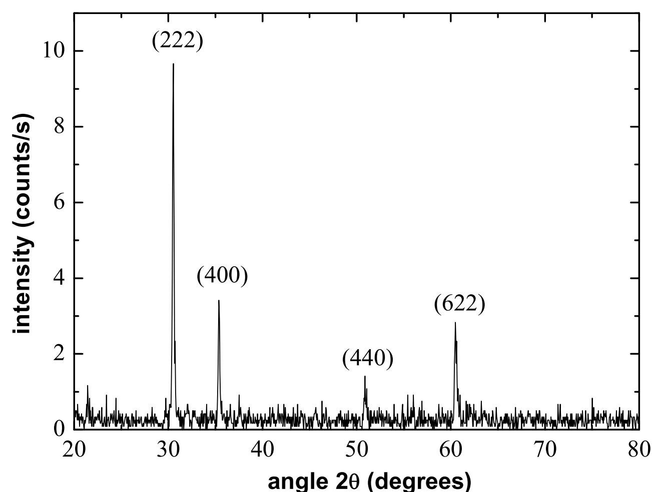

Figure 3. X-ray diffraction patterns in grazing geometry (6°) for an ITO film grown by PED at 500 °C on a single-crystal *c*-cut sapphire substrate.

phenomenon. A good fit (as shown in figure 1) may only be obtained by decreasing the oxygen concentration. More precisely, the best fit was obtained assuming that the ITO film is composed of: (i) a stoichiometric ITO surface layer with a 24 nm thickness; (ii) an sub-oxide underlayer (118 nm), in which the oxygen composition varies between 2.23 (just beneath the stoichiometric surface layer) and 2.48 at the interface with the substrate. It can thus be concluded that a mean value for the oxygen composition can be estimated to be 2.35, i.e. with an overall composition $(In_{1.8}Sn_{0.2})O_{2.35}$, meaning that a film with a strong oxygen deficiency has been formed in these conditions.

All the ITO films grown under the low oxygen pressure used in this work were found to present the same oxygen deficiency whatever the film thickness or nature of the substrate. In addition, the near surface region of the ITO films (about 20 nm), presenting an enriched oxygen concentration with respect to the bulk, was observed whatever the substrate used and its thickness slightly increases with the growth temperature.

3.2. Film structure

All the ITO films grown at $T < 200\,^{\circ}\mathrm{C}$ were found to be amorphous, the *in situ* crystallization occurring during growth at higher T. Figure 2 represents a typical diffraction pattern recorded for a film grown on *c*-cut sapphire at 500 °C (190 nm). The peaks on this diagram correspond to the (222) and (400) reflections of the ITO structure and to their harmonics. The angular positions of these peaks correspond to those of the stoichiometric ITO compound. This initially appears surprising, as a large oxygen deficiency could lead to noticeable changes of the axis parameters in the case of oxides [16]. Moreover no diffraction peaks which could be due to the presence of sub-oxides of indium (InO or In_2O) or tin (SnO), or even to metallic Sn or In, in the films are observed. To further study the possible presence of such phases, a study of the XRD in grazing incidence was carried out. The corresponding diagram is presented in figure 3, and only shows the characteristic peaks of the ITO material. The sole structural phase identified in the films is thus the ITO stoichiometric phase, despite the large oxygen deficiency in the films. We have thus to conclude that amorphous forms or microcrystallites are present in the films together with the stoichiometric oxide phase, i.e. heterogeneous oxide films are formed in these conditions. In figure 3 (grazing incidence) the ratio of the (222) to (400) peak intensity, $I(222)/I(400) \approx 3$, corresponds to perfectly random crystallite orientation of ITO grains, while in figure 2 (Bragg–Brentano geometry), the value of this ratio (0.25) indicates that some of the crystallites present a preferential textured growth, with the (400) ITO planes parallel to the substrate surface. The rocking curve of the (400) diffraction line was measured and is given in the inset in figure 2. A FWHM value around 1° demonstrates a rather low mosaicity and a possible epitaxy.

To check the formation of epitaxial films, pole figures were recorded for ITO films on *c*-cut sapphire grown at 300 and 500 °C, and poles were only observed for films grown at 500 °C. Figures 4(a) and (b) represent the pole figures of the (440) (at $2\theta = 51.04°$) and (222) (at $2\theta = 30.581°$) planes of ITO. In figure 4(a), 12 poles can be observed, located at a declination angle Ψ equal to 45°, i.e. the value expected for the (440) poles of ITO crystallites presenting the (400) texture. In addition, figure 4(a) shows three poles located at a Ψ value of 57.6° corresponding to the poles of the (02.4) planes of sapphire substrates ($2\theta = 52.56°$). The respective azimuthal positions of the (440) ITO and (02.4) sapphire poles lead to the following in-plane epitaxial relationships between ITO film and sapphire substrate:

$$[\bar{1}10]_{\mathrm{ITO}} \parallel [11.0]_{c-\mathrm{S}} \quad \text{and} \quad [110]_{\mathrm{ITO}} \parallel [1\bar{1}.0]_{c-\mathrm{S}}$$

with 'ITO' and '*c*-S' representing the ITO film and the *c*-cut sapphire substrate, respectively.

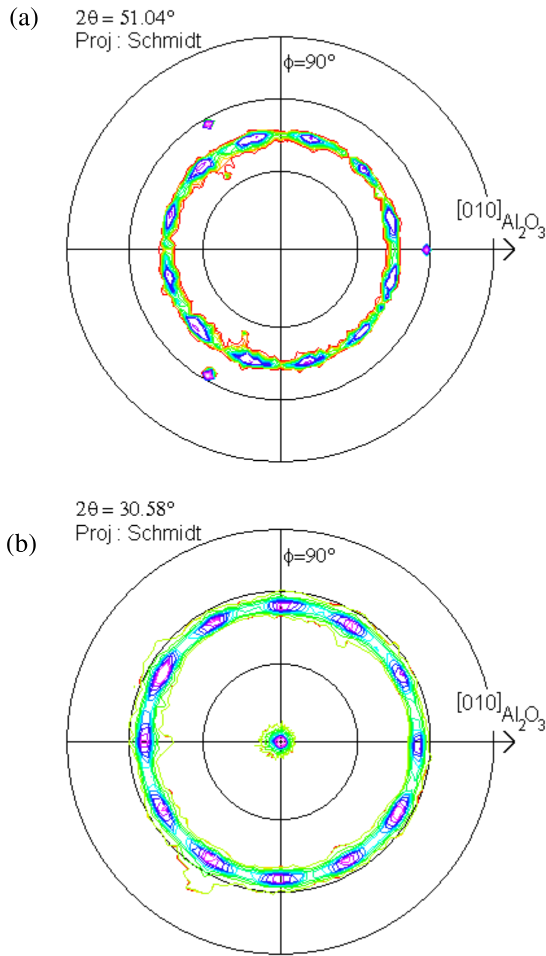

Figure 4. Pole figures of the (440) (a) and (222) (b) ITO family planes or a ITO film grown by PED at 500 °C on a single-crystal *c*-cut sapphire substrate.

In figure 4(a), (440) poles which could be related to the presence of ITO (222) oriented crystallites are not observed. Such (222) oriented crystallites would have given rise to poles at a declination angle Ψ equal to 35.3°, and no poles are observed at this location in figure 4(a). This point was further checked by measurements of the pole figure of the (222) ITO planes presented in figure 4(b). A central pole is observed, corresponding to the (222) crystallites with their [222] direction normal to the *c*-cut sapphire, in agreement with figure 2, but poles which would appear at a declination Ψ equal to 70.5° are not present in this figure. Moreover, figure 4(b) shows 12 poles at a declination angle Ψ equal to 54.7°, i.e. the value expected for (222) poles of ITO crystallites presenting the (400) orientation of a cubic structure, on *c*-cut sapphire substrate. The azimuthal positions of these poles correspond to those expected in the framework of the epitaxial relationships deduced from figure 4(a).

The in-plane arrangement leading to the epitaxial relationships is schematically presented in figure 5. In this schema, the *c*-cut sapphire is represented by the characteristic hexagons of the (0001) basal plane. The ITO plane in the schema is represented with the square symmetry of the

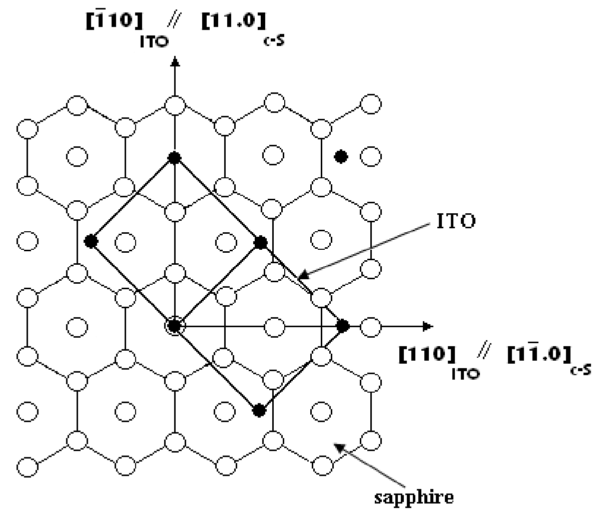

Figure 5. Schematic description of the epitaxial relationship between the hexagonal sapphire substrate and cubic ITO film.

(400) plane. With the in-plane parameters of the square and hexagon unit of the two lattices (0.476 nm for the sapphire and 1.0118 nm for ITO), a very important lattice mismatch is deduced. However, the specific orientation of the film on the substrate can be explained in the framework of the domain matching epitaxy or extended atomic distance mismatch approach [17], in which m lattice units of the film match with p lattice units of the substrate. The values of m and p are defined as the minimum integers which satisfy the following relation:

$$md_{\mathrm{f}} \approx pd_{\mathrm{s}} \qquad \text{or} \qquad [d_{\mathrm{f}}/d_{\mathrm{s}}] \approx [p/m],$$

d_{f} and d_{s} being the respective atomic distances in the film and substrate parallel directions. The corresponding lattice mismatch δ can thus be defined by

$$\delta = 2[md_{\mathrm{f}} - pd_{\mathrm{s}}]/[md_{\mathrm{f}} + pd_{\mathrm{s}}].$$

The atomic distances d_{f} (1.4309 nm) and d_{s} (0.824 nm) along the $[\bar{1}10]_{\mathrm{ITO}}$ and $[11.0]_{c-\mathrm{S}}$ directions respectively, are such that $4d_{\mathrm{f}} \approx 7d_{\mathrm{s}}$, and the lattice mismatch along this common direction is $\delta = 0.77\%$. In the same way, considering the alignment of the $[110]_{\mathrm{ITO}}$ with the $[1\bar{1}.0]_{c-\mathrm{S}}$ directions, the d_{f} (1.4309 nm) and d_{s} (0.476 nm) values are such that the following domain lattice mismatch is established: $d_{\mathrm{f}} \approx 3d_{\mathrm{s}}$, leading to $\delta = 0.2\%$. These low values of lattice mismatch along the two directions clearly justify the epitaxial relationships observed in this work.

3.3. Thin film properties

The ITO films grown at $T < 300$ °C are amorphous, insulating, and present a large oxygen deficiency. In contrast, the ITO films obtained at $T > 300$ °C are crystalline, greatly absorbing and show measurable room T resistivity. The transport properties of these latter films were thus investigated through resistivity measurements as a function of temperature, $R(T)$.

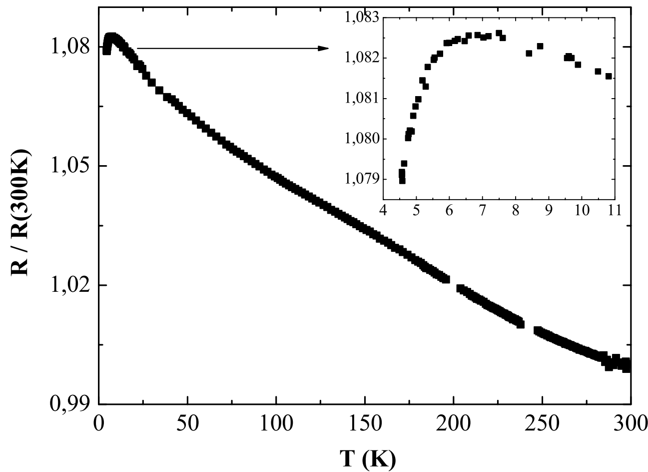

Figure 6. Temperature dependence of the normalized resistance $R(T)/R$ (300 K) curve (room T to liquid He T) for the ITO films grown on a single-crystal *c*-cut sapphire substrate at 300 °C. In the inset is presented the beginning of the superconducting transition.

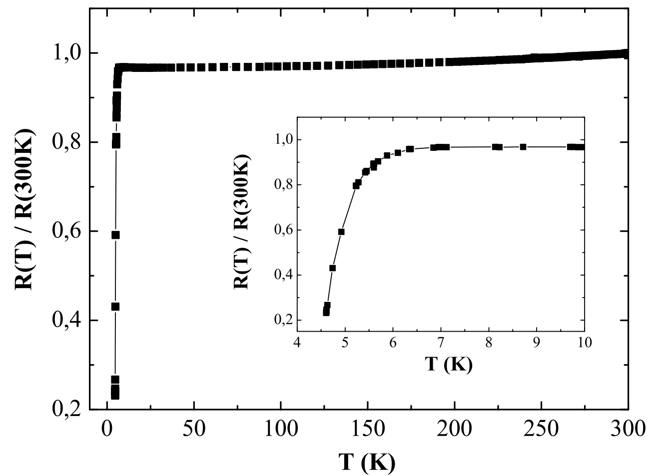

Figure 7. Temperature dependence of the normalized resistance $R(T)/R$ (300 K) curve (room T to liquid He T) for the ITO films grown on a single-crystal *c*-cut sapphire substrate at 500 °C. In the inset is presented the detailed superconducting transition.

Figure 6 represents the typical variation of the film resistance with T for an ITO film grown at 300 °C (150 nm). From room T down to about 6 K, this curve shows characteristic semiconductor behaviour. Then a decrease in resistivity begins to be observed (see the inset in figure 6), and could be attributed to a superconducting transition in a fraction of the film. Figure 7 represents the $R(T)$ curve for an ITO films grown at 500 °C (190 nm), and characterizes a metallic behaviour over the whole temperature range. Then at low T, a clear superconducting transition is observed with a T_c onset equal to 6 K. This transition is not complete (zero resistivity is not reached), meaning that one part of the film is not in the superconducting state.

These films are heterogeneous (see above), with at least two phases, one being a stoichiometric and crystalline oxide phase, in which a sub-oxide and/or metallic phase is embedded; the $R(T)$ curve in figure 6 could thus be explained by the electrical conductivity in the sub-oxide (due to the large oxygen deficiency). The low T superconducting transition which begins to be observed could be related to the presence of a low concentration of metallic clusters in the film. For increasing growth temperature (figure 7), the $R(T)$ curve could be explained by the electrical conductivity through metallic clusters which can further present a superconducting transition at low T. A rather similar behaviour has been observed in the case of indium/indium oxide thin film composites, in which a superconducting transition is observed, due to the presence of the indium metallic clusters [18–20].

The superconducting transition temperature T_c (6 K) is an interesting indication of the nature of the metallic clusters. Indeed, this value is higher than the T_c values of bulk In (T_c = 3.4 K) and Sn (T_c = 3.5 K). The difference from the experimental value could be related to the T_c increase with decreasing size of the clusters. However, results reported did not show a large increase in T_c with decrease in the size of the clusters [21, 22]. The T_c value (6 K), could thus be indicative of the presence of clusters of an In and Sn alloy, as the T_c value of these compounds can reach value as high as 6.5 K for a compound with the InSn composition [23].

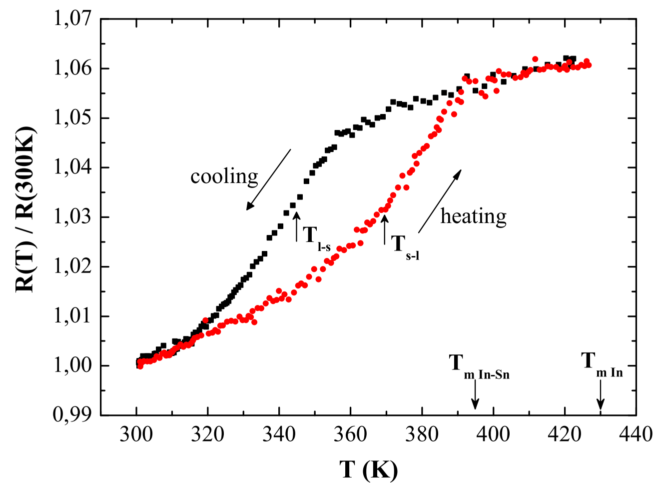

Figure 8. Temperature dependence of the normalized resistance $R(T)/R$ (300 K) curve (room T to 450 K) for ITO film grown at 500 °C.

To check the presence of such In–Sn clusters in the ITO films, we have studied the resistivity behaviour of these films in the room T to 180 °C range. Indeed, the In–Sn metallic clusters which are in the solid state at room T would undergo a solid to liquid phase transition at a melting temperature T_m which would be lower than that of In (430 K), since the presence of Sn would depress the melting temperature, as has been measured [24]. Moreover, the In–Sn compound resistivity in the liquid state being higher than that in the solid state [24], an increase in the resistance of the film should be observed during the heating from room T up to 450 K. This increase in resistivity is associated with the solid–liquid state transition in the In–Sn clusters.

This is indeed observed, as can be seen in figure 8. A clear increase of the resistance occurs at T around 350 K, and

then a linear increase in the resistivity regime is reached at about 390 K. Such a curve can thus be interpreted in terms of the solid–liquid transition of In–Sn clusters at T_m about 370 K. For comparison purposes, the melting temperature of pure In (430 K) and InSn alloy in bulk form (395 K) are also indicated in this figure. Whatever the precise composition of the clusters, and therefore whatever their bulk melting point, a noticeable decrease of this melting point is observed in the clusters. Moreover during the cooling down of the ITO film (from 430 to 300 K), a hysteresis is clearly evidenced on the $R(T)$ curve, i.e. the solidification (freezing) temperature (around 345 K) is lower than the melting temperature (about 370 K).

This behaviour, i.e. a strong decrease of the melting temperature and the presence of a hysteresis cycle, which clearly separates melting and solidification temperatures, has been reported in the studies of the temperature evolution of nanoparticles [25]. For example, In nanoparticles showed a large melting point depression (110 K) for a 2 nm particle radius [26]. The depression of the melting point has been analysed and modelled [27], and a variation inversely proportional to the particle size (down to a few nanometres) has been established. When nanoparticles are embedded in a matrix, a depression of the melting point can be observed [25], as well as a superheating of nanoparticles [28, 29], i.e. a melting point higher than the T_m bulk value. In the case of In in porous silica glass (about 6 nm pore size), a hysteresis loop was observed with a melting point depression, i.e. T_m of about 385 K [30]. In contrast, In clusters in the 15–20 nm range obtained by ion implantation in SiO_2 can be superheated about 13 K above the bulk T_m value [31].

The reason is that the melting point of embedded nanoparticles depends on, in addition to their size, the nature of the nanoparticle–matrix interface. Various theoretical analyses and models based on classical thermodynamics arguments have been proposed for predicting the melting temperature of spherical nanoparticles embedded in a matrix [25, 29, 32, 33]. These models show that the T_m value will depend upon the values of σ_{lm} and σ_{sm}, the liquid and solid particle–matrix interfacial energies, which are related to the contact angle between the liquid nucleus and the solid matrix [29, 32, 33]. Owing to the fact that these interfacial energy terms contain structural and chemical components, the difference between the absolute values of T_m and T_f in the various studies should be related to the differences in nature and structure of the matrix. For example in the case of In nanoparticles in Al samples prepared by rapid quenching from the melt [25] and by ball milling of In and Al mixtures [29], differences in melting point were observed with a superheating for the melt quenched ones, and a melting point depression for the ball milled ones. These differences have been attributed to the existence of a coherent (or semicoherent) interface between the nanoparticles and the matrix leading to superheating, while a random interface is associated with melting point depression [29].

The comparison of these results with those reported in this paper, indicates that despite the crystalline matrix, the In–Sn metallic clusters do not develop coherent interfaces with this matrix, and accordingly a melting point depression is observed. On the other hand, it is not possible to deduce a precise value for the size of the In–Sn clusters; a rough estimation should be of the order of a few nanometres, to explain the value of the melting point depression.

4. Discussion

Indium tin oxide films with a large oxygen deficiency (more than 20%) have been formed by PED, and the analysis of their crystalline structure and transport properties leads to the conclusion that they are nanocomposite films with metallic In–Sn clusters embedded in a crystalline and stoichiometric oxide matrix. It is then possible to propose a plausible scenario for the formation of such nanocomposite oxide films during the *in situ* growth of oxygen deficient ITO films. In the growth conditions of the PED used in this work, the ITO films are formed with a large oxygen deficiency: $(In_{1.8}Sn_{0.2})O_{2.4}$. Then, a pertinent parameter determining the nature, structure, microstructure and properties of such sub-oxide thin films will be the substrate temperature. At room T, homogeneous amorphous and insulating thin films are formed, but with increasing growth temperature (300 °C), oxygen deficient ITO film will start to crystallize *in situ*. In such a system, the most stable oxide phases are the stoichiometric phases rather than the other sub-oxide phases (InO, In_2O or SnO). We can thus assume that stoichiometric ITO crystallizes at the expense of the remaining sub-oxide. In this framework, the transformation of oxygen deficient ITO films can be schematically described by the following disproportionation reaction:

$$(In_{1.8}Sn_{0.2})O_{2.4} \rightarrow a(In_{1.8}Sn_{0.2})O_3 + b(In_{1.8}Sn_{0.2})O_{2.4-x}$$

with x characterizing the increasing oxygen deficiency of the sub-oxide, and

$$a = x/(0.6 + x) \qquad \text{and} \qquad b = 0.6/(0.6 + x)$$

determining the respective fraction of phases. In this description, $0 < x \leqslant 2.4$, and the limit value for x (2.4) corresponds to the formation of In–Sn clusters in a stoichiometric ITO matrix.

The presence of a highly oxygen deficient material in the film, i.e. $(In_{1.8}Sn_{0.2})O_{2.4-x}$, would induce electrical conductivity in the films, as is observed through the semiconducting behaviour observed in figure 6. At this intermediate 300 °C temperature, the fraction of metallic (In–Sn) clusters would certainly be low, and would only give rise to the superconducting transition which begins to be observed (figure 6). At a higher temperature (500 °C), the transformation of the oxygen deficient ITO films would be more complete (figure 7), i.e. the stoichiometric phase would grow at the expense of the sub-oxide and in the extreme case, the sub-oxide completely disappears according to the following disproportionation reaction:

$$(In_{1.8}Sn_{0.2})O_{2.4} \rightarrow 0.8(In_{1.8}Sn_{0.2})O_3 + 0.2(In_{1.8}Sn_{0.2}).$$

This extreme situation leads to the formation of metallic clusters (In–Sn) embedded in a stoichiometric oxide matrix.

In this framework, metallic conductivity will be present in the films through the metallic InSn clusters (and electron tunnelling between clusters), followed by a superconducting transition in these metallic clusters at a lower temperature.

In this approach, there is the disproportionation of the oxygen deficient ITO films into a nanocomposite film by crystallization of a stoichiometric oxide matrix with a metallic nanometric phase. This process appears rather similar to that recently reported for the disproportionation reaction in understoichiometric gallium oxide films [34], leading to the formation of a crystalline stoichiometric Ga_2O_3 phase, and a Ga_2O_{3-x} phase with enhanced oxygen deficiency responsible for the electrical conductivity of the films [34]. In these two cases (sub-oxides of gallium and ITO), the disproportionation reaction is due to the presence of metastable insulating sub-oxide phases, which under a thermal activation, transformed into heterogeneous multiphase systems with a stable stoichiometric oxide phase and a more oxygen deficient sub-oxide phase (the case of gallium oxide or ITO at 300 °C) or a metallic phase (ITO at 500 °C).

In this framework, in addition to the temperature, the driving force for the disproportionation reaction is the oxygen deficiency in the ITO films. By controlling precisely this oxygen deficiency during the PED growth, it would be possible to control the concentration of metallic clusters in the films grown at 500 °C. Accordingly, the transport and optical properties of the films would thus be tuned from purely transparent and insulating to absorbing and metallic like films. Moreover, this phenomenon being already observed in indium tin and gallium sub-oxide films could certainly be applied to other oxides whose sub-oxides are known to be not stable. This could give rise to new and interesting transport properties.

5. Summary

In summary, we have shown that nanocomposite ITO thin films can be grown by *in situ* pulsed-electron beam deposition, through a disproportionation reaction induced by a strong oxygen deficiency. The very specific transport properties associated with the presence of metallic clusters in an insulating stoichiometric oxide matrix could allow some applications. For example a local heating with a laser beam could induce the disproportionation reaction leading to the formation of conducting lines. In the same way the large differences in optical properties related to the presence or absence of metallic nanoparticles could be used in non-volatile storage devices.

Acknowledgments

The authors gratefully acknowledge financial support from the Hubert Curien Partnership PAI Brâncusi no. 14762ZH and the Romanian Ministry for Education and Research, project numbers 12-112/2008 and PN 09.39.03.01.

References

[1] Hamberg I and Grandquist C G 1986 *J. Appl. Phys.* **60** R123
[2] Tahar R B H, Bau T, Ohya Y and Takahashi Y 1998 *J. Appl. Phys.* **83** 2631
[3] Hamberg I, Grandquist C G, Berggren K F, Sernelius B E and Engstroom L 1984 *Phys. Rev.* B **30** 3240
[4] Ederth J, Johnsson P, Niklasson G A, Hoel A, Hultåker A, Heszler P, Granqvist C G, van Doorn A R, Jongerius M J and Burgard D 2003 *Phys. Rev.* B **68** 155410
[5] Wu Y, Maree C H M, Haglund R F Jr, Hamilton J D, Morales Paliza M A, Huang M B, Feldman L C and Weller R A 1999 *J. Appl. Phys.* **86** 991
[6] Morales-Paliza M A, Haglund R F Jr and Feldman L C 2002 *Appl. Phys. Lett.* **80** 3757
[7] Mori N 1993 *J. Appl. Phys.* **73** 1327
[8] Wang R X, Beling C D, Fung S, Djurisic A B, Ling C C, Kwong C and Li S 2005 *J. Phys. D: Appl. Phys.* **38** 2000
[9] Zhu F, Huan C H A, Zhang K and Wee A T S 2000 *Thin Solid Films* **359** 244
[10] Nistor M, Mandache N B and Perrière J 2008 *J. Phys. D: Appl. Phys.* **41** 165205
[11] Chaudhary R J, Ogale S B, Shinde S R, Kulkani V N, Venkatesan T, Harshavardhan K S, Strikovski M and Hannoyer B 2004 *Appl. Phys. Lett.* **84** 1483
[12] Nistor M, Gherendi F, Mandache N B, Ioachim A, Banciu M G, Nedelcu L and Alexandru H V 2005 *Appl. Surf. Sci.* **247** 169
[13] Nistor M and Mandache N B 2005 *J. Optoelectron. Adv. Mater.* **7** 1619
[14] Gonzalo J, Afonso C N and Perrière J 1995 *Appl. Phys. Lett.* **67** 1325
[15] Gonzalo J, Afonso C N and Perrière J 1996 *J. Appl. Phys.* **79** 8042
[16] Perez-Casero R, Perrière J, Gutierrez-Llorente A, Defourneau D, Millon E, Seiler W and Soriano L 2007 *Phys. Rev.* B **75** 165317
[17] Narayan J, Dovidenko K, Sharma A K and Oktyabarsky S 1998 *J. Appl. Phys.* **84** 2597
[18] Fiory A T, Hebrard A F and Glaberson W I 1983 *Phys. Rev.* B **28** 5075
[19] Gammel P L, Hebrard A F and Bishop D J 1988 *Phys. Rev. Lett.* **60** 144
[20] Kwon C, Kim J, Lee H J, Jung H C and Park C G 1991 *J. Appl. Phys.* **69** 6716
[21] Li W H, Yang C C, Tsao F C, Wu S Y, Huang P J, Chung M K and Yao Y D 2005 *Phys. Rev.* B **72** 214516
[22] Graf M J, Huber T E and Huber C A 1992 *Phys. Rev.* B **45** 3133
[23] Merriam M F and Von Herzen M 1963 *Phys. Rev.* **131** 637
[24] Shen R R, Zu F Q, Xi Y, Li X F, Ding G H and Liu H M 2006 *Phys. Scr.* **73** 184
[25] Sheng H W, Lu K and Ma E 1998 *Acta Mater.* **46** 5195
[26] Zhang M, Efremov M Yu, Schiettekatte F, Olson E A, Kwan A T, Lai S L, Wisleder T, Greene J E and Allen L H 2000 *Phys. Rev.* B **62** 10548
[27] Buffat Ph and Borel J P 1976 *Phys. Rev.* A **13** 2287
[28] Xu Q, Sharp I D, Yuan C W, Yi D O, Liao C Y, Glaeser A M, Minor A M, Beeman J W, Ridgway M C, Kluth P, Ager J W, Chrzan D C and Haller E E 2006 *Phys. Rev. Lett.* **97** 155701
[29] Lu K and Jin Z H 2001 *Curr. Opin. Solid State Mater. Sci.* **5** 39
[30] Unruh K M, Huber T E and Huber C A 1993 *Phys. Rev.* B **48** 9021
[31] Tagliente M A, Mattei G, Tapfer L, Vittori Antisari M and Mazzoldi P 2004 *Phys. Rev.* B **70** 075418
[32] Caupin F 2008 *Phys. Rev.* B **77** 184108
[33] Zhong J, Jin Z H and Lu K 2001 *J. Phys.: Condens. Matter* **13** 11443
[34] Nagarajan L, De Souza R A, Samuelis D, Valov I, Börger A, Janek J, Becker K D, Schmidt P C and Martin M 2008 *Nat. Mater.* **7** 391